INRIA

UNITÉ DE RECHERCHE
INRIA-SOPHIA ANTIPOLIS

Institut National
de Recherche
en Informatique
et en Automatique

Domaine de Voluceau
Rocquencourt
B.P.105
78153 Le Chesnay Cedex
France

Tél. (1) 39 63 55 11

Rapports de Recherche

N° 690

EXPLICIT CALCULATION OF REACTIVE FLOWS WITH AN UPWIND FINITE ELEMENT HYDRODYNAMICAL CODE

Abderhaman HABBAL
Alain DERVIEUX
Hervé GUILLARD
Bernard LARROUTUROU

JUIN 1987

Un schéma en éléments finis décentrés pour le calcul d'écoulements réactifs

Explicit calculation of reactive flows with an upwind finite-element hydrodynamical code

A. HABBAL, A. DERVIEUX, H. GUILLARD, B. LARROUTUROU

INRIA Sophia-Antipolis
Avenue Émile Hugues
Sophia Antipolis
06565 VALBONNE

RESUME

Ce travail présente une première étape dans la mise au point de méthodes numériques pour le calcul d'écoulements réactifs avec flammes minces dans des géométries complexes. Nous avons retenu dans ce but une approche de type éléments finis avec maillage non structuré à cause de sa simplicité de mise en oeuvre dans des géométries complexes, et des possibilités qu'elle offre pour des techniques d'adaptation de maillage. De plus, la méthode numérique choisie se caractérise par l'utilisation d'une approximation spatiale décentrée afin d'en accroître la robustesse. Le présent rapport présente en détail la méthode numérique ainsi que son application à quelques problèmes modèles de propagation de front de flammes.

ABSTRACT

The present work is a preliminary step in the construction of a numerical method for the computation of reactive flows with thin flames in complex geometries. For this purpose, a finite element type approximation on non-structured meshes is chosen, because of its capacity to handle complex geometries, and to accept mesh adaptation procedures without huge modifications of the numerical code. In addition the spatial approximation uses an upwind scheme to improve the robustness of the method. The present report describes in detail the numerical algorithm and its application to some flame propagation model problems.

Table of contents

1. INTRODUCTION

This paper deals with the approximation of compressible reactive flows ; this field has been rather developed in the last ten years and has reached the level at which applications involving complex geometries and complex solutions, with local strong gradients, can be considered.

A possible approach for the solution of problems presenting these two features is the combination of **non-structured meshes** with **adaptive methods** : non-structured meshes can be useful for complex geometries, and their combination with mesh adaptation is easy to handle because data structures are not restrictive.

Starting from this point of view, the computation will be performed with **irregular meshes**, in the following sense : the topology is irregular ("unstructured"), and the metrics are irregular (local stretching, large or small angles).

The use of such irregular grids requires a robust discrete approximation. We present in this paper a method which uses a Galerkin **finite-element** approximation for the parabolic terms, an **upwind** mixed finite-element finite-volume approximation for the first-order hyperbolic terms, and an explicit time stepping. The FEM (Finite Element Method) approach is well adapted to non structured meshes ; when using conformal simplicial element (triangles, tetrahedra) the use of local grid refinement by element subdivisions is more easy (see [11], [12]); furthermore, mesh distorsion is rather well accepted by FEM approximations. Lastly, the introduction of upwinding still improves the robustness of FEM when very irregular meshes are used. The "upwind FEM" approach presented in this paper has already been intensively used for non reacting flows in two- and three-dimensional geometries, combined or not with mesh adaptation (see [7], [8], [13], [15]).

In this paper, this method is applied to some simplified model problems of flame propagation in compressible gaseous mixtures. The main simplification concerns the chemical model : a simple one-step reaction $R \longrightarrow P$ is considered. In addition, an inviscid Euler model is used instead of the full compressible Navier-Stokes equations.

The purpose of the calculations is to study the unsteady and steady behaviours of two-dimensional flames. Similar computations have also been performed by several authors using finite-difference or finite-volume methods ; we refer among other recent works to Amsden et al [1], [2], Gosman [9] and O'Rourke and Amsden [14].

After recalling the governing equations and their nondimensionalization in Section 2, we describe in detail the numerical method in Section 3 and then present several results illustrating the robustness of the method in Section 4.

2. GOVERNING EQUATIONS

We consider the two-dimensional flow of a reacting gaseous mixture, with the assumption of a single one-step chemical reaction $R \longrightarrow P$. Moreover,we will neglect the gas viscosity for simplicity. We therefore write the dimensionalized governing equations in the form (see [18]):

$$\rho_t + (\rho u)_x + (\rho v)_y = 0 \tag{2.1}$$

$$(\rho u)_t + (\rho u^2 + p)_x + (\rho uv)_y = 0 \tag{2.2}$$

$$(\rho v)_t + (\rho uv)_x + (\rho v^2 + p)_y = 0 \tag{2.3}$$

$$E_t + [u(E+p)]_x + [v(E+p)]_y = \lambda \Delta T + Q\omega \tag{2.4}$$

$$(\rho Y)_t + (\rho Y u)_x + (\rho Y v)_y = \rho D \Delta Y - m\omega \tag{2.5}$$

with

$$E = \rho C_v T + \frac{1}{2}\rho(u^2 + v^2) \tag{2.6}$$

$$p = (\gamma - 1)\rho C_v T, \quad \gamma = C_p/C_v \tag{2.7}$$

$$\omega = B\frac{\rho Y}{m} exp\ (-\frac{\mathcal{E}}{R^o T}) \tag{2.8}$$

We have used classical notations : ρ is the mixture density, u and v are the components of the velocity $\overrightarrow{U}$, p is the pressure, E is the sum of the thermal and kinetic energies per unit volume, λ is the mixture thermal conductivity, T the temperature, Q the heat released by the chemical reaction and ω is the rate at which this reaction proceeds. Moreover, Y is the mass fraction of the reactant R, D is its molecular diffusion coefficient, and m is the molecular mass of the reactant. Lastly, C_p and C_v are the constant pressure and constant volume specific heats of the mixture, γ is the specific heat ratio, B is the Arrhenius prefactor, $\mathcal{E}$ is the activation energy of the mixture and R^o denotes the universal gas constant. We classically assume that the quantities $\lambda, Q, \rho D, C_p, C_v, \gamma, B$ and $\mathcal{E}$ are constant.

The above equations are associated to initial data for the five variables $\rho, \rho u, \rho v, E, \rho Y$, and to boundary conditions which depend on the flow geometry (see Section 3 below).

In a pratical way, we solve instead of (2.1) – (2.8) a nondimensionalized form of this set of equations. We then consider a time unit t_0, a length unit l_0, temperature and mass

fraction units T_0 and Y_0, and a density unit ρ_0. We also refer the velocity to $u_0 = \frac{l_0}{t_0}$, and the pressure and energy to $p_0 = E_0 = \rho_0 u_0^2$.

We can then introduce the following nondimensional parameters [$(\rho D)_0$ denotes the constant value of ρD] :

$$\mathcal{L}e = \frac{\lambda}{(\rho D)_0 C_p} \quad \text{(Lewis number);}$$

$$PR = \frac{l_0 u_0 \rho_0 C_p}{\lambda}$$

(for a viscous fluid PR would be the product of the Prandtl number $Pr = \frac{C_p \mu}{\lambda}$ by the Reynolds number $Re = \frac{l_0 u_0 \rho_0}{\mu}$, μ denoting the gas viscosity) ;

$$\mathcal{M}a = \frac{u_0}{\sqrt{(\gamma - 1) C_p T_0}} \quad \text{(Mach number);}$$

$$\mathcal{Q} = \frac{Q Y_0}{m u_0^2} \quad \text{(nondimensional heat release);}$$

$$N = \frac{\mathcal{E}}{R^0 T_0} \quad \text{(nondimensional activation energy);}$$

$$A = B\ t_0 \quad \text{(nondimensional Arrhenius prefactor).}$$

With these notations, the normalized governing equations write :

$$\rho_t + (\rho u)_x + (\rho v)_y = 0 \tag{2.9}$$

$$(\rho u)_t + (\rho u^2 + p)_x + (\rho u v)_y = 0 \tag{2.10}$$

$$(\rho v)_t + (\rho u v)_x + (\rho v^2 + p)_y = 0 \tag{2.11}$$

$$E_t + [u(E+p)]_x + [v(E+p)]_y = \frac{\Delta T}{(\gamma - 1)\mathcal{M}a^2 PR} + \mathcal{Q}\Omega \tag{2.12}$$

$$(\rho Y)_t + (\rho Y u)_x + (\rho Y v)_y = \frac{\Delta Y}{\mathcal{L}e PR} - \Omega \tag{2.13}$$

with

$$T = \gamma(\gamma - 1)\mathcal{M}a^2 \frac{1}{\rho} [E - \frac{1}{2}\rho(u^2 + v^2)] \tag{2.14}$$

$$\gamma \mathcal{M}a^2 p = \rho T \tag{2.15}$$

$$\Omega = A\ \rho\ Y\ exp(-\frac{N}{T}). \tag{2.16}$$

The numerical treatment of these equations is detailed in the next section.

Before concluding this section, let us be more specific about the solutions of (2.9) – (2.13) which will be considered. We are essentially interested in slow combustion phenomena, as those arising in flame propagation problems. We will consider a flame front propagating in a fresh gaseous mixture of density ρ_u, temperature T_u and mass fraction Y_u (here the subscript u stands for "unburnt"). For an isobaric combustion, the burnt gases have the density $\rho_b = \rho_u \frac{T_u}{T_b}$ (the subscript stands for "burnt") from the equation of state (2.15), T_b being the hot gases temperature, and contain no reactant : $Y_b = 0$.

The hot gas temperature T_b can be deduced from the energy equation (2.12) rewritten in terms of temperature :

$$\rho T_t + \rho u T_x + \rho v T_y = \frac{\Delta T}{PR} + Ma^2(\gamma - 1)\mathcal{Q}\Omega + Ma^2(\gamma - 1)(p_t + up_x + vp_y) \tag{2.17}$$

which leads to :

$$T_b = T_u + Ma^2(\gamma - 1)\mathcal{Q}Y_u.$$

The speed and the thickness of this flame can then be evaluated using the classical "high activation energy asymptotics" (see [4],[5]). We get :

$$V_f = \sqrt{\frac{2A\mathcal{L}e}{PR}}\sqrt{\frac{T_u}{T_b}}\sqrt{\frac{1}{\rho_u}}exp(-\frac{N}{2T_b})\frac{T_b}{N}\frac{T_b}{(T_b - T_u)}$$

for the flame velocity, and :

$$L_f = \frac{1}{PRV_f\rho_u}$$

for the flame thickness. It may be interesting to compare the flame speed V_f to the maximal sound speed $V_s = \frac{\sqrt{T_b}}{Ma}$ in the hot gases, to get an idea of a Mach number based on the flame propagation velocity.

Such a flame propagation problem is therefore defined by the following parameters :

$$\gamma,\ \rho_u,\ Y_u,\ T_u,\ T_b,\ Ma,\ PR,\ \mathcal{L}e,\ \mathcal{Q},\ A,\ N,$$

(in our calculations, we classically take $\gamma = 1.4$, and choose the mass fraction and temperature units so that $Y_u = T_u = 1$).

3. NUMERICAL SCHEME

The numerical scheme used to solve equations (2.9)-(2.13) is mainly based on the following remark:

All the terms in the left-hand side of equations (2.9)-(2.12) exactly form the classical Euler equations describing a two-dimensional inviscid non reacting gas flow. Compared to the system of the Euler equations, our system (2.9)-(2.13) contains three types of additional terms: the diffusive terms (ΔY and ΔT), the reactive terms ($\mathcal{Q}\Omega$ and $-\Omega$), and the terms describing the convection of the reactant ($(\rho Y u)_x$ and $(\rho Y v)_y$).

In order to provide a robust treatment of the hydrodynamical terms, our scheme is based on an Euler solver involving some characteristic upwind finite-volume spatial approximation. In particular, this scheme has the capability to accurately compute acoustic or shock waves (see [7], [8]). The remaining terms are evaluated using a P1 finite-element approximation: this approximation is appropriate for the diffusion and reaction terms, and reveals to be adequate for treating the convection of the reactant (due to the importance of molecular diffusion effects).

Another way of presenting this scheme, which we now detail, is to say that a finite-volume approach is used for the hydrodynamical variables $\rho, \rho u, \rho v, E$ and that a finite-element approximation is used for the reactant separate density ρY.

3.1. Temporal differencing

The simple (first-order accurate) Euler explicit scheme is used to advance in time the numerical solution.

The time step Δt with which the scheme operates is then to be chosen according to the following classical stability conditions, where $U = \|\vec{U}\| = \sqrt{u^2+v^2}$ denotes the gas velocity, $c = \sqrt{\gamma \frac{p}{\rho}}$ the local sound speed, and where Δh is some measure of the mesh spacing:

* Stability condition for the hydrodynamical terms (Euler equations) and for the convection of reactant:

$$\frac{\Delta t}{\Delta h}\, max(|U+c|, |U|, |U-c|) = CFL_1 \leq 1 \tag{3.1}$$

* Stability restriction for the diffusive terms:

$$\frac{2\Delta t}{\Delta h^2}\, max(\frac{\gamma}{\rho PR}, \frac{1}{\rho PR\mathcal{L}e}) = CFL_2 \leq 1 \tag{3.2}$$

which comes from equations (3.17)-(3.18) below and from the following form of the energy equation:

$$E_t + [u(E+p)]_x + [v(E+p)]_y = \frac{\gamma}{PR}\Delta(\frac{E}{\rho}) - \frac{\gamma}{2PR}\Delta(u^2+v^2) + \mathcal{Q}\Omega \tag{3.3}$$

In all our calculations, the stability restriction for the reactive terms is much less severe than the conditions (3.1) and (3.2), and therefore is not taken into account.

3.2. Spatial differencing for the hydrodynamical variables

As mentioned before, a finite-volume approach is used for the hydrodynamical variables $\rho, \rho u, \rho v, E$. In order to present this approximation, let us first rewrite equations (2.9)-(2.12) in the following form:

$$\left\{\begin{array}{l} \frac{\partial}{\partial t}W + \frac{\partial}{\partial x}F_1(W) + \frac{\partial}{\partial y}F_2(W) + \frac{\partial}{\partial x}R_1(W,W_x) + \frac{\partial}{\partial y}R_2(W,W_y) + H(W) = 0 \\ \\ W = \begin{pmatrix} \rho \\ \rho u \\ \rho v \\ E \end{pmatrix} = (W^{(k)})_{k=1,4} \\ \\ F_1(W) = \begin{pmatrix} \rho u \\ \rho u^2 + p \\ \rho uv \\ u(E+p) \end{pmatrix}, \quad F_2(W) = \begin{pmatrix} \rho u \\ \rho uv \\ \rho v^2 + p \\ v(E+p) \end{pmatrix} \\ \\ R_1(W,W_x) = \begin{pmatrix} 0 \\ 0 \\ 0 \\ -D_T T_x \end{pmatrix}, \quad R_2(W,W_y) = \begin{pmatrix} 0 \\ 0 \\ 0 \\ -D_T T_y \end{pmatrix}, \quad H(W) = \begin{pmatrix} 0 \\ 0 \\ 0 \\ -\mathcal{Q}\Omega \end{pmatrix} \end{array}\right. \tag{3.4}$$

We have set:

$$D_T = \frac{1}{(\gamma-1)\mathcal{M}a^2 PR}; \tag{3.5}$$

moreover, we will use the notations:

$$\underline{F} = \begin{pmatrix} F_1(W) \\ F_2(W) \end{pmatrix}, \quad \underline{R} = \begin{pmatrix} R_1(W,W_x) \\ R_2(W,W_y) \end{pmatrix} \tag{3.6}$$

Let $\mathcal{D}$ be the computational domain, Γ its boundary and $\vec{n}$ the outward unit normal on Γ. The boundary Γ will be divided into two parts Γ_1 and Γ_2 on which different types of boundary conditions will be used. We assume that $\mathcal{D}$ is a polygonal bounded domain of $\Re^2$, and call $\mathcal{T}_h$ a standard finite-element triangulation of $\mathcal{D}$.

For every vertex S_i $(i = 1, \ldots n_h)$ of $\mathcal{T}_h$, we define the control volume $\hat{S}_i$ as follows: every triangle having S_i as a vertex is divided into six subtriangles using the median lines; the cell $\hat{S}_i$ is the union of the resulting subtriangles having S_i as a vertex (see Fig. 1). We shall denote $\partial\hat{S}_i$ the boundary of $\hat{S}_i$ and $\vec{\nu}_i = (\nu_{ix}, \nu_{iy})$ the outward unit normal on $\partial\hat{S}_i$.

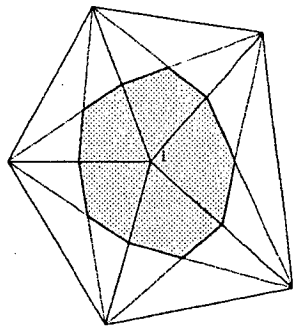

Fig. 1 : Cell $\hat{S}_i$

The discrete equations are obtained by integrating the governing equations (3.4) on each control volume $\hat{S}_i$. Using Green's formula we obtain :

$$\begin{aligned} \iint_{\hat{S}_i} (W^{n+1} - W^n) dx dy \; &+ \Delta t \int_{\partial \hat{S}_i} \underline{F}(W^n).\overrightarrow{\nu}_i \, d\sigma \\ &+ \Delta t \int_{\partial \hat{S}_i} \underline{R}(W^n).\overrightarrow{\nu}_i \, d\sigma \\ &+ \Delta t \iint_{\hat{S}_i} H(W^n) dx dy \; = 0. \end{aligned} \tag{3.7}$$

We now have to define the numerical evaluation of the integrals in (3.7).

♣ *Temporal and source terms*

For the temporal and source terms, we use the simple one point formula :

$$\begin{cases} \iint_{\hat{S}_i} (W^{n+1} - W^n) dx dy &= area(\hat{S}_i)(W_i^{n+1} - W_i^n) \\ \iint_{\hat{S}_i} H(W^n) dx dy &= area(\hat{S}_i) H(W_i^n) \end{cases} \tag{3.8}$$

◇ *Convective terms*

The integration of the convective terms is performed by the characteristic first-order upwind scheme briefly described below (see [7] for more details):

The boundary $\partial \hat{S}_i$ of the cell $\hat{S}_i$ is splitted into bisegments $\partial \hat{S}_{ij}$ joining the middle of the segment S_iS_j to the centroids of the two triangles having S_i and S_j as common vertices: $\partial \hat{S}_{ij} = \overrightarrow{G_1 I_{ij}} + \overrightarrow{I_{ij} G_2}$ (see Fig. 2).

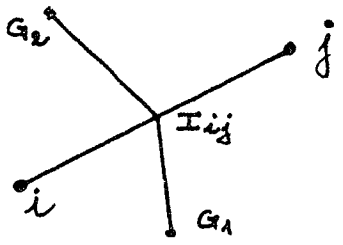

Fig. 2

Calling $\kappa(i)$ the set of neighboring nodes of S_i, we have : $\partial\hat{S}_i = \sum_{S_j \in \kappa(i)} \partial\hat{S}_{ij}$. Then we have:

$$\begin{cases} \int_{\partial\hat{S}_i} \underline{F}(W^n).\vec{\nu_i}\, d\sigma = \sum_{j\in\kappa(i)} \int_{\partial\hat{S}_{ij}} \underline{F}(W^n).\vec{\nu_i}\, d\sigma & < 1 > \\ \quad + \int_{\partial\hat{S}_i\cap\Gamma_1} \underline{F}(W^n).\vec{n}\, d\sigma & < 2 > \\ \quad + \int_{\partial\hat{S}_i\cap\Gamma_2} \underline{F}(\overline{W}^n).\vec{n}\, d\sigma & < 3 > \end{cases} \tag{3.9}$$

The approximation of the boundary terms $< 2 >$ and $< 3 >$ will be defined in a subsequent section. The first term of the right-hand side of (3.9) is integrated as follows:

$$\int_{\partial\hat{S}_{ij}} \underline{F}(W^n).\vec{\nu_i}\, d\sigma = \Phi_{ij}(W_i^n, W_j^n), \tag{3.10}$$

where Φ is the numerical flux function. In this study we have used, following Van Leer, the Q-scheme whose numerical flux function is defined by (see [8]):

$$\Phi_{ij}^{VL}(U,V) = \frac{1}{2}\left(\underline{F}(U) + \underline{F}(V)\right) \int_{\partial\hat{S}_{ij}} \vec{\nu_i} + \frac{1}{2}|P_{ij}\left(\frac{U+V}{2}\right)|(U-V). \tag{3.11}$$

with:

$$P_{ij}(U) = \frac{\partial F_1}{\partial U}(U).\int_{\partial\hat{S}_{ij}} \nu_{ix}\, d\sigma + \frac{\partial F_2}{\partial U}(U).\int_{\partial\hat{S}_{ij}} \nu_{iy}\, d\sigma. \tag{3.12}$$

(We emphasize that this upwind scheme is *not* the well known "Van Leer's splitting" scheme [16].)

♡ *Diffusive terms*

To evaluate the integral of the diffusive terms:

$$\int_{\partial\hat{S}_i} \underline{R}(W^n).\vec{\nu_i}\, d\sigma = -D_T \int_{\partial\hat{S}_i} \nabla T^n.\vec{\nu_i}\, d\sigma, \tag{3.13}$$

we need to define the value of the gradient of the temperature along each cell boundary. This is done by considering that the temperature T^n is given in each triangle of $\mathcal{T}_h$ by a P1 interpolation. Therefore $\underline{R}$ is constant on each triangle τ and the integral (3.13) reduces to:

$$\begin{cases} \sum\limits_{\tau \in \mathcal{T}(i)} \underline{R}_\tau . \int\limits_{\partial \hat{S}_i \cap \tau} \vec{\nu_i}\, d\sigma, & < 1 > \\ + \int\limits_{\partial \hat{S}_i \cap \Gamma_1} \underline{R}(W^n).\vec{n}\, d\sigma & < 2 > \\ + \int\limits_{\partial \hat{S}_i \cap \Gamma_2} \underline{R}(\overline{W}^n).\vec{n}\, d\sigma & < 3 > \end{cases} \tag{3.14}$$

where $\mathcal{T}(i)$ is the set of triangles having S_i as a vertex and where $\underline{R}_\tau$ denotes the constant value of $\underline{R}$ in a triangle τ of $\mathcal{T}_h$. The approximation of the boundary terms $< 2 >$ and $< 3 >$ will be made precise below.

REMARK: This evaluation of the diffusive terms is equivalent to a P1 finite-element approximation of the Laplace operator. Indeed, if ϕ_i is the classical P1 finite-element basis function associated to the vertex S_i, the constant value of $\nabla\phi_i$ in a triangle $\tau \in \mathcal{T}(i)$ is exactly:

$$\nabla\phi_i|_\tau = -\frac{1}{area(\tau)}(\overrightarrow{I_{ij}G_\tau}^{\perp} + \overrightarrow{G_\tau I_{il}}^{\perp}) = -\frac{1}{area(\tau)} \int\limits_{\partial \hat{S}_i \cap \tau} \vec{\nu_i}\, d\sigma, \tag{3.15}$$

where $\overrightarrow{I_{ij}G_\tau}^{\perp}$ and $\overrightarrow{G_\tau I_{il}}^{\perp}$ are the outward normals on $\partial \hat{S}_i \cap \tau$ (see Fig. 3).

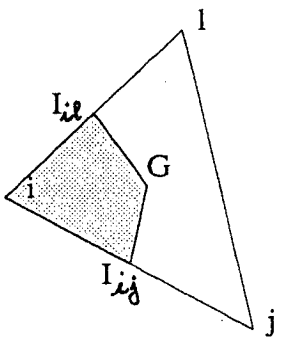

Fig. 3

We then observe that (3.14) $< 1 >$ is the usual finite-element discretization of ΔT:

$$< 1 >= -\sum_{\tau \in \mathcal{T}(i)} \iint_\tau \underline{R}.\nabla\phi_i\, dx\, dy = D_T \sum_{\tau \in \mathcal{T}(i)} \iint_\tau \nabla T.\nabla\phi_i\, dx\, dy\ . \tag{3.16}$$

3.3. Spatial differencing for the mass fraction variable

Two different discretizations of equation (2.13) for the mass fraction will be considered:

♠ *Non-conservative formulation*

The following equation in non-conservative form can be deduced from (2.9) and (2.13):

$$\rho Y_t + \rho u Y_x + \rho v Y_y = D_Y \Delta Y - \Omega \tag{3.17}$$

with:

$$D_Y = \frac{1}{\mathcal{L}ePR}. \tag{3.18}$$

Our non conservative treatment of the mass fraction variable consists in using a P1 mass-lumped finite-element approximation of (3.17). The fifth independent variable is therefore $W_5 = Y$, given by the expression $Y = \sum_i Y_i \phi_i$, where ϕ_i is the usual P1 finite-element basis function associated with the vertex S_i. The discrete equations are obtained by multiplying (3.17) by a P1 basis function ϕ_i and integrating in $\mathcal{D}$:

$$\begin{aligned}
\iint_{\mathcal{D}} \rho^n (Y^{n+1} - Y^n)\phi_i \, dx \, dy = &-\Delta t \iint_{\mathcal{D}} \nabla Y^n . (\rho \vec{U})^n \phi_i \, dx \, dy && < 1_1 > \\
&- \Delta t D_Y \iint_{\mathcal{D}} \nabla Y^n . \nabla \phi_i \, dx \, dy && < 1_2 > \\
&- \Delta t \iint_{\mathcal{D}} \Omega^n \phi_i \, dx \, dy && < 1_3 > \\
&+ \Delta t D_Y \int_{\Gamma_1} \nabla Y^n . \vec{n} \, \phi_i d\sigma && < 2 > \\
&+ \Delta t D_Y \int_{\Gamma_2} \nabla \overline{Y}^n . \vec{n} \, \phi_i d\sigma && < 3 >
\end{aligned} \tag{3.19}$$

We shall deal with the approximation of the boundary terms $< 2 >$ and $< 3 >$ in the following section.(3.19) can be rewritten as:

$$\left\{
\begin{aligned}
\sum_{\tau \in \mathcal{T}(i)} \iint_{\tau} \rho^n (Y^{n+1} - Y^n)\phi_i \, dx \, dy = &-\Delta t \Big(\sum_{\tau \in \mathcal{T}(i)} \nabla Y^n|_\tau . \iint_{\tau} (\rho \vec{U})^n \phi_i \, dx \, dy \Big) \\
&- \Delta t D_Y \Big(\sum_{\tau \in \mathcal{T}(i)} \nabla \phi_i|_\tau . \nabla Y^n|_\tau \, area(\tau) \Big) \\
&- \Delta t \Big(\sum_{\tau \in \mathcal{T}(i)} \iint_{\tau} \Omega^n \, \phi_i \, dx \, dy \Big) \\
&+ \text{boundary terms} ,
\end{aligned}
\right. \tag{3.20}$$

and the description of the discrete equations is completed by the following quadrature formulas for the numerical evaluation of the integrals in (3.20) (including the mass-lumped approximation for the time-derivative term):

$$\begin{cases} \iint_\tau \rho^n (Y^{n+1} - Y^n)\phi_i \, dx \, dy & \approx \frac{1}{3} area(\tau) \rho_i^n (Y_i^{n+1} - Y_i^n) \\ \iint_\tau (\rho \overrightarrow{U})^n \phi_i \, dx \, dy & \approx \frac{1}{3} area(\tau) (\rho \overrightarrow{U})_i^n \\ \iint_\tau \Omega^n \phi_i \, dx \, dy & \approx \frac{1}{3} area(\tau) \Omega_i^n \end{cases} \tag{3.21}$$

♣ *Conservative formulation*

We will also consider a conservative discretization of the mass fraction equation (2.13). In this conservative version, the fifth independent variable is $W_5 = \rho Y$, and the discrete equations follow from a mass-lumped finite-element discretization of the equation (2.13) in conservative form:

$$\begin{aligned} \iint_D (W_5^{n+1} - W_5^n)\phi_i \, dx \, dy = {} & \Delta t \iint_D \frac{W_5^n}{\rho^n} (\rho \overrightarrow{U})^n . \nabla \phi_i \, dx \, dy && < 1_1 > \\ & - \Delta t D_Y \iint_D \nabla (\frac{W_5^n}{\rho^n}) . \nabla \phi_i \, dx \, dy && < 1_2 > \\ & - \Delta t \iint_D \Omega^n \phi_i \, dx \, dy && < 1_3 > \\ & - \Delta t \int_{\Gamma_1} (\rho \overrightarrow{U})^n . \overrightarrow{n} \frac{W_5^n}{\rho^n} \phi_i \, d\sigma && < 2_1 > \\ & + \Delta t D_Y \int_{\Gamma_1} \phi_i \nabla (\frac{W_5^n}{\rho^n}) . \overrightarrow{n} \, d\sigma && < 2_2 > \\ & - \Delta t \int_{\Gamma_2} \phi_i \overline{(\rho \overrightarrow{U})}^n . \overrightarrow{n} \frac{\overline{W_5}^n}{\overline{\rho}^n} \, d\sigma && < 3_1 > \\ & + \Delta t D_Y \int_{\Gamma_2} \phi_i \nabla (\frac{\overline{W_5}^n}{\overline{\rho}^n}) . \overrightarrow{n} \, d\sigma && < 3_2 > \end{aligned} \tag{3.22}$$

The evaluation of the boundary terms $< 2 >$ and $< 3 >$ will be described in the sequel. The mass-lumped approximation is again used for the left-hand side and for the term $< 1_3 >$ of (3.22):

$$\begin{cases} \iint_D (W_5^{n+1} - W_5^n)\phi_i \, dx \, dy &= ((W_5^{n+1})_i - (W_5^n)_i) \int_D \phi_i \, dx \, dy \\ \iint_D \Omega^n \phi_i \, dx \, dy &= \Omega_i^n \int_D \phi_i \, dx \, dy \end{cases} \tag{3.23}$$

The diffusive term $< 1_2 >$ of (3.22) is evaluated as in (3.20), i.e. by considering that the gradient of $Y = \frac{W_5}{\rho}$ is constant in each triangle. Lastly, the convective term $< 1_1 >$ is computed according to the formulas:

$$\begin{cases} \iint_D Y^n (\rho \vec{U})^n . \nabla \phi_i \, dx \, dy &\approx \sum_{\tau \in \mathcal{T}(i)} \nabla \phi_1|_\tau . \iint_\tau (\rho \vec{U})^n Y^n \, dx \, dy \\ \iint_\tau \rho \vec{U} Y \, dx \, dy &\approx \frac{area(\tau)}{3} [(\rho \vec{U} Y)_i + (\rho \vec{U} Y)_j + (\rho \vec{U} Y)_l] \end{cases} \tag{3.24}$$

where in the last formula (S_i, S_j, S_k) are the three vertices of the triangle τ.

3.4. Boundary conditions

We will consider two types of boundary conditions on the boundary $\Gamma = \Gamma_1 \cup \Gamma_2$: Γ_1 denotes the part of the boundary which represents a wall of the vessel in which the flame propagates, while Γ_2 represents an inflow or an outflow boundary.

◇ *Boundary conditions on a wall*

We will essentially consider only the case of adiabatic slipping walls. Thus, on Γ_1:

$$\frac{\partial T}{\partial n} = \frac{\partial Y}{\partial n} = \vec{U} . \vec{n} = 0. \tag{3.25}$$

Therefore, the term $< 2 >$ of equation (3.14) vanishes, while the term $< 2 >$ in (3.9) becomes:

$$\int_{\partial \hat{S}_i \cap \Gamma_1} \underline{F}(W^n) . \vec{n} \, d\sigma = \int_{\partial \hat{S}_i \cap \Gamma_1} \begin{pmatrix} 0 \\ p.n_x \\ p.n_y \\ 0 \end{pmatrix} d\sigma \tag{3.26}$$

Note that in this procedure, the slip condition is applied in a weak variational way, as in cell-centered finite-volume formulations.

In the equations (3.19) or (3.22) for the mass fraction, all boundary terms $< 2 >$ on Γ_1 vanish.

♡ *Inflow or outflow boundary conditions*

The numerical evaluation of the term $< 3 >$ of (3.9) representing inflow or outflow boundary conditions for the hydrodynamical variables is less simple; it is based on a characteristic upwinding applied at these boundaries; we refer to [15] for more details.

We assume zero diffusive fluxes at the inflow or outflow boundaries (in the calculations reported below, the inflow or outflow boundary Γ_2 always represents far open ends of an infinitely long open tube): thus, the term $< 3 >$ of (3.14), the term $< 3 >$ in (3.19) and the term $< 3_2 >$ of (3.22) vanish.

For the remaining term representing the reactant inflow or outflow on Γ_2 (term $< 3_1 >$ in (3.22)), we use a Dirichlet condition for an inflow boundary ($\overline{Y} = Y_\infty$ given) and simply set $\overline{W_5} = (W_5)_i$ if the vertex S_i is located on an outflow boundary.

4. NUMERICAL RESULTS

We have considered two types of physical problems: several experiments of premixed flame propagation in a closed vessel, and a flame propagating in an open rectangular tube. For all these experiments, we have used the following values for the physico-chemical parameters defining the phenomenon:

ρ_u	Y_u	T_u	T_b	Ma	PR	$\mathcal{L}e$	$\mathcal{Q}$	A	N
1.3	1.	1.	5.	0.04	10.	1.	6250.	4.10^6	40.

With these values, the (asymptotic) laminar flame velocity is 1., the flame thickness is equal to 0.0766, while the ratio of the sound speed in the burnt gases to the flame velocity is about 55.

4.1. Flames propagating in a closed vessel

4.1.1. A 1-D like computation

In this section we study the one-dimensional propagation of a flame in a closed tube. Similar computations are reported for example by Westbrook [17] and Kooker [10].

4.1.1.1. Physical problem

We consider the one-dimensional propagation of a flame in a closed adiabatic rectangular vessel. The dimension of the chamber is 1. x 0.1 and the initial conditions are chosen to simulate a flame moving inside the tube. They write:

For $x < 0.68$ (fresh mixture):

$$(2_1) \begin{cases} \rho = \rho_u \\ T = T_u \\ Y = Y_u \end{cases}$$

For $x \geq 0.70$ (burnt gases):

$$(2_2) \begin{cases} \rho = \rho_b \\ T = T_b \\ Y = Y_b \end{cases}$$

For $0.68 \leq x \leq 0.70$ the density and mass fraction vary linearly between the two above states (we recall that $\rho_b = \rho_u \frac{T_u}{T_b}$ and $Y_b = 0.$). In addition, the gas is considered to be initially at rest and at constant pressure.

4.1.1.2. Discretization

Triangulation

Since the physical problem has a one-dimensional solution, we have considered triangulations consisting of only two rows of elements in the y direction. Two triangulations have been considered : T_1 is a regular 61x3 mesh having 183 vertices and 240 triangles,

while T_2 is a regular 121x3 mesh with 363 vertices and 480 triangles. These triangulations are generated using an isotropic pattern (Union Jack flag like) to avoid symmetry problems.

Choice of the time step

The time step is chosen according to the first stability restriction (3.1), with $CFL_1 = 0.50$ on the coarse mesh T_1 and $CFL_1 = 0.25$ on the fine mesh T_2 (the value $CFL_1 = 0.50$ could not be used with the T_2 mesh because of the diffusive stability condition (3.2)).

4.1.1.3. Results

Our purpose in considering this 1D-like computation is to compare the conservative and non-conservative versions of the code. We will assume that the fine mesh results are accurate enough to play the role of the exact results.

The computation with the coarse mesh and conservative version has been performed till complete consumption of the reactant and pressure uniformisation. The combustion is complete at t=0.3044. The maximum flame velocity is about 4.5 times the asymptotic flame velocity at the temperature T_b.

The results at t=0.055 (400 time steps for the coarse mesh, 1550 for the fine one) are presented for the comparison of the conservative and non-conservative code (Figs. 1.1.1 to 1.1.3). The main conclusion of this comparison is that the discrepancies between the conservative and non conservative codes often overpass the differences between the coarse and fine mesh computations. This shows that conservativeness is an important feature for accuracy, even in this example where the solution does not exhibit very sharp gradients.

REMARK: On the other hand, the non-conservative formulation has the following advantage: the time step Δt can be chosen in order to insure that the numerical values of the mass fraction Y remain in the interval [0.,1.] (discrete maximum principle). Such is not strictly the case with the conservative code, where Y is obtained as the ratio of the variables W_5 and W_1. Despite of this argument, we have found it preferable to use the conservative formulation.

4.1.2. A tilted flame in a closed tube

4.1.2.1. Physical problem

We now consider a closed rectangular combustion chamber $R_2 = [0,1]\text{x}[0,0.166]$ with adiabatic slipping walls. At t=0 an initial pseudo-flame is defined as follows:

For $x + y < 0.68$

$$(2_1) \begin{cases} \rho = \rho_u \\ T = T_u \\ Y = Y_u \end{cases}$$

For $x + y \geq 0.70$

$$(2_2) \begin{cases} \rho = \rho_b \\ T = T_b \\ Y = Y_b \end{cases}$$

For $0.68 \leq x+y \leq 0.70$ the density and mass fraction quantities vary linearly between the two above states.
As in Section 4.1.1 the gas is considered to be initially at rest and at uniform pressure. Therefore the initial conditions are the same than in Section 4.1.1 except that the initial pseudo-flame is tilted with an angle of 45^o.

4.1.2.2. Discretization

For this 2-D computation, we use a regular 61 x 11 mesh T_3 with 671 vertices and 1200 triangles and with $\Delta x = \Delta y$. The time step is defined by $CFL_1 = 0.5$.

4.1.2.3. Results

Figures 1.2.1 and 1.2.2 display the evolution of the velocity field and mass fraction contours. The flame presents a nearly plane configuration after t=0.08. This corresponds to a motion of about twice its thickness, which shows that the adjustement of the flame is very rapid. The appearance of weak but undesirable oscillations in the velocity field at the wall can be noticed on the second plot in Fig. 1.2.1. This fact is also illustrated by the wall temperature distribution shown in Fig. 1.2.3. We recall that the boundary conditions at the wall are imposed via pressure integrals (see (3.26)) and therefore does not imply the strict nullity of the normal velocities on the wall.

4.1.3. A flame in a square vessel

4.1.3.1. Physical problem

A further investigation of 2-D and wall effects is performed with the following configuration: in a square chamber $S_1 = [0, 0.5]^2$ an initial pseudo-flame is defined as in Section 4.1.2 except that the transition is now located in the slice $0.08 < x + y < 0.10$. This configuration simulates an initial square pseudo-flame in a larger square vessel (Fig. 1.3.1).

4.1.3.2. Discretization

We again use two different triangulations, which are both regular with $\Delta x = \Delta y$: a 31 x 31 mesh T_4 with 961 vertices and 1800 triangles and a finer 51 x 51 mesh T_5 of 2601 vertices and 5000 triangles.
The time step is driven by: $CFL_1 = 0.50$ on T_4 and $CFL_1 = 0.25$ on T_5.

4.1.3.3. Results

Figures 1.3.2 to 1.3.4 display the evolution of the flame computed on the coarser mesh. After t=0.04 the flame presents a quasi-spherical configuration and then, after interaction with the walls, turns to be concave. The total consumption of the reactant is achieved at t=0.15.

Figure 1.3.5 shows the reactant density contours and velocity field computed on the fine mesh at the same time as for Fig. 1.3.2. The fine and coarse mesh results are in very good agreement, although the numerical scheme is only first-order accurate in space and

time. This conclusion is confirmed by Fig. 1.3.6 that displays the walls distribution of horizontal velocity, density and reactant density at the same time as the previous figure. The CPU time ratio between the two computations is about 2.

4.1.4. An ignited flame in a square vessel

4.1.4.1. Physical problem

We consider now the previous square vessel S_1 filled with an uniformly unburnt gas defined by the values (2_1) of Section 4.1.1.1. The gas is initially at rest and at constant pressure. At t=0 the adiabatic flame temperature T_b is imposed on a small part of the upper wall in order to ignite the mixture and initiate a flame. The walls are considered as slipping boundaries and adiabatic, except in the small portion of the upper wall where the temperature is maintained constant and equal to the adiabatic flame temperature T_b during the computation.

4.1.4.2. Discretization

We again use the triangulation T_4 and a CFL number of 0.5.

4.1.4.3. Results

Figures 1.4.1 to 1.4.4 show the evolution of the mass fraction contours and velocity field during the computation. Due to the rather small heating segment, the flame begins to develop slowly. However note that the ignition of the flame is accompagnied by very large velocities. These rather large velocities are computed by the numerical scheme with only slight oscillations. Then the flame develops a quasi-spherical shape centered on the heating portion of the upper wall. After interacting with the vertical walls the flame propagates downward while flattening.

4.2. An anchored flame in a open tube

4.2.1. Physical problem

In this section we consider a rectangular tube with open extremities. The walls of this tube are assumed to be adiabatic, except on a small portion of the upper wall where the adiabatic flame temperature T_b is imposed. At the left end of the tube, a uniform flow of unburnt gases is imposed, with a velocity equal to 5. In order to compare the development of the anchored flame with the propagation of a planar flame, a flame is initially established downwind the hot part of the upper wall (see the first plot in Fig. 2.1).

4.2.2. Discretization

The triangulation used for this problem is the T_3 triangulation already used in Section 4.1.2. The values of the variables in the far field medium used in the upwind boundary conditions at the inflow boundary (resp: outflow boundary) are the values (2_1) of the fresh gases (resp: the values (2_2) of the burnt gases) defined in Section 4.1.1.1..

4.2.3. Results

Figure 2.1 displays the evolution of the isotherms. After some time, one can observe that the initial pseudo-flame moves to the right and finally goes out of the tube, while a second flame develops from the hot part of the upper wall. As the fresh gases cannot cross this hot point without burning, an anchored flame is obtained. The convergence history presented in Fig. 2.2 shows that a steady state is reached.

5. CONCLUSION

The method described in this paper allows the study of a class of combustion problems in which the characteristic time-scales involved in the physical phenomenon are not too different. Several applications are presented, including unsteady flames propagating in tubes or in closed vessels and an anchored steady flame.

Several points still need some improvements in order to treat more stiff problems. In particular, several investigations which have been carried out for the basic Euler solver (see [6], [8], [12]) are currently extended to the treatment of reactive flows (see [3]): extension of implicit formulations to low Mach number flows, development of more accurate explicit approximations for the investigation of acoustics-combustion interaction, as well as the study of mesh adaptation procedures for a low-cost and accurate calculation of thinner flames.

This research program is felt as a further step towards the ultimate objective of these studies, which is to qualify the presented scheme to solve combustion problems involving complex geometries and stiff solutions.

ACKNOWLEDGEMENTS

We are indebted to our colleague F. Fezoui who kindly provided the Euler solver used in this work.

REFERENCES

[1] A. A. AMSDEN, J. D. RAMSHAW, P. J. O'ROURKE, J. K. DUKOWICZ, " KIVA: A computer program for two- and three-dimensional fluid flows with chemical reactions and fuel sprays", Los Alamos National Laboratory Report LA-10245-MS, (1985).

[2] A. A. AMSDEN, J. D. RAMSHAW, P. J. O'ROURKE, J. K. DUKOWICZ, "Improvements and extensions of the KIVA computer program" , Los Alamos National Laboratory Report LA-10534-MS, (1985).

[3] F. BENKHALDOUN, A. DERVIEUX, G. FERNANDEZ, H. GUILLARD, B. LARROUTUROU, "Some investigations of finite-element solutions to stiff combustion problems: mesh adaptation and implicit time stepping", NATO advanced research workshop on "Combustion modelling and its applications", Lyon, France, April 1987.

[4] W. B. BUSH, F. E. FENDELL, " Asymptotic analysis of laminar flame propagation for general Lewis numbers", Comb. Sci. and Tech. **1**, p 421, (1970).

[5] P. CLAVIN, "Dynamic behavior of premixed flame fronts in laminar and turbulent flows", Prog. Energy Combust. Sci. **11**, p. 1, (1985).

[6] J. A. DESIDERI, A. GOUDJO, V. SELMIN, "Third-order numerical schemes for hyperbolic problems", INRIA Report 607, (1987).

[7] F. FEZOUI, "Résolution des équations d'Euler par un schéma de Van Leer en éléments finis", INRIA Report 358, (1985).

[8] F. FEZOUI, B. STOUFFLET, "A class of implicit upwind schemes for Euler simulation with unstructured meshes", submitted to J. Comp. Phys..

[9] A. D. GOSMAN, "Aspects of the simulation of combustion in reciprocating engines", "Numerical simulation of combustion phenomena", Glowinski Larrouturou Temam eds., Lecture Notes in Physics, **241**, p. 46, Springer-Verlag, (1985).

[10] D. E. KOOKER, "Numerical predictions for laminar flame propagation in confined ozone/oxygen mixtures: Influence of initial temperature and pressure", AIAA paper 79-0292, (1979).

[11] R. LOHNER, K. MORGAN, J. PERAIRE, O. C. ZIENKIEWICZ, "Recent developments in FEM-CFD, "The free-Lagrange method", Fritts Crowley Trease eds., p. 236, Lecture notes in physics, **238**, Springer-Verlag, (1985).

[12] B. PALMERIO, "Self adaptive FEM algorithms for the Euler equations", INRIA Report 338, (1984).

[13] B. PALMERIO, A. DERVIEUX, "Application of a finite-element moving node adaptive method to accurate shock capturing", First Int. Conf. on "Numerical grid generation in computational fluid dynamics", Landshut, Federal Republic of Germany, August 1987.

[14] P. J. O'ROURKE, A. A. AMSDEN, "Implementation of a conjugate residual iteration in the KIVA computer program", to appear.

[15] B. STOUFFLET, J. PERIAUX, F. FEZOUI, A. DERVIEUX, "Numerical simulation of 3-D hypersonic Euler flow around space vehicle using adapted finite elements", AIAA paper 87-0560, (1987).

[16] B. VAN LEER, "Flux-vector splitting for the Euler equations", "Eighth international conference on numerical methods in fluid dynamics", Krause ed., p. 507, Lecture notes in physics, **170**, Springer-Verlag, (1982).

[17] C. K. WESTBROOK, "A generalized ICE method for chemically reactive flows in combustion systems", J. Comp. Phys., **29**, p. 67, (1978).

[18] F. A. WILLIAMS, "Combustion Theory", Benjamin-Cummings, second edition, (1985).

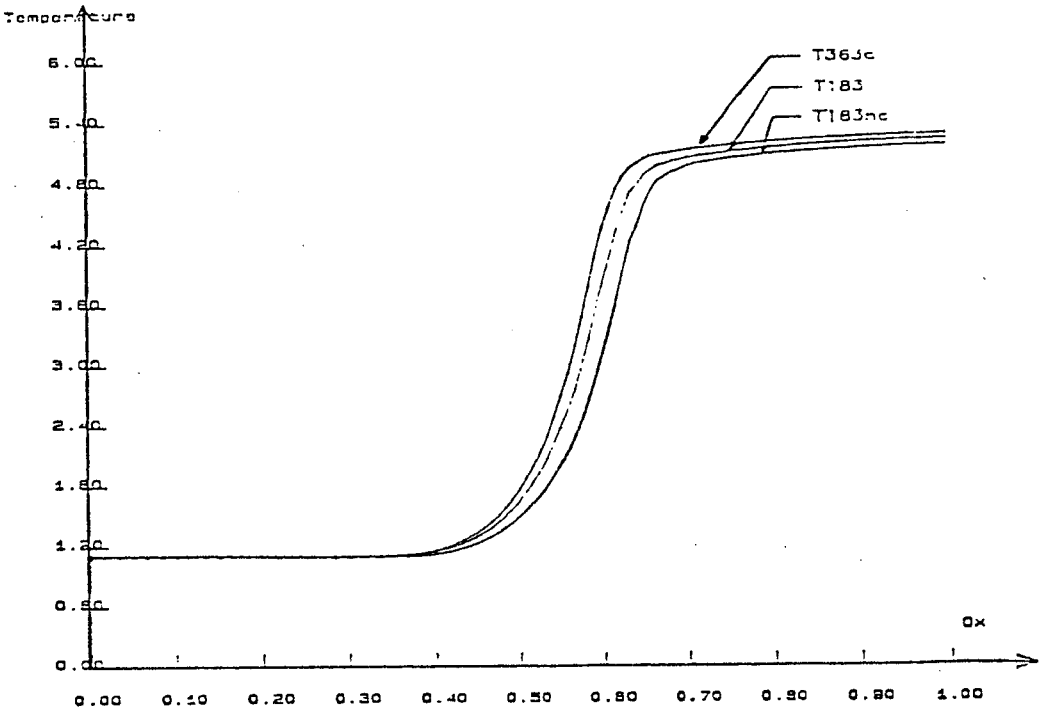

Figure 1.1.1. : Temperature profile at t = 0.055

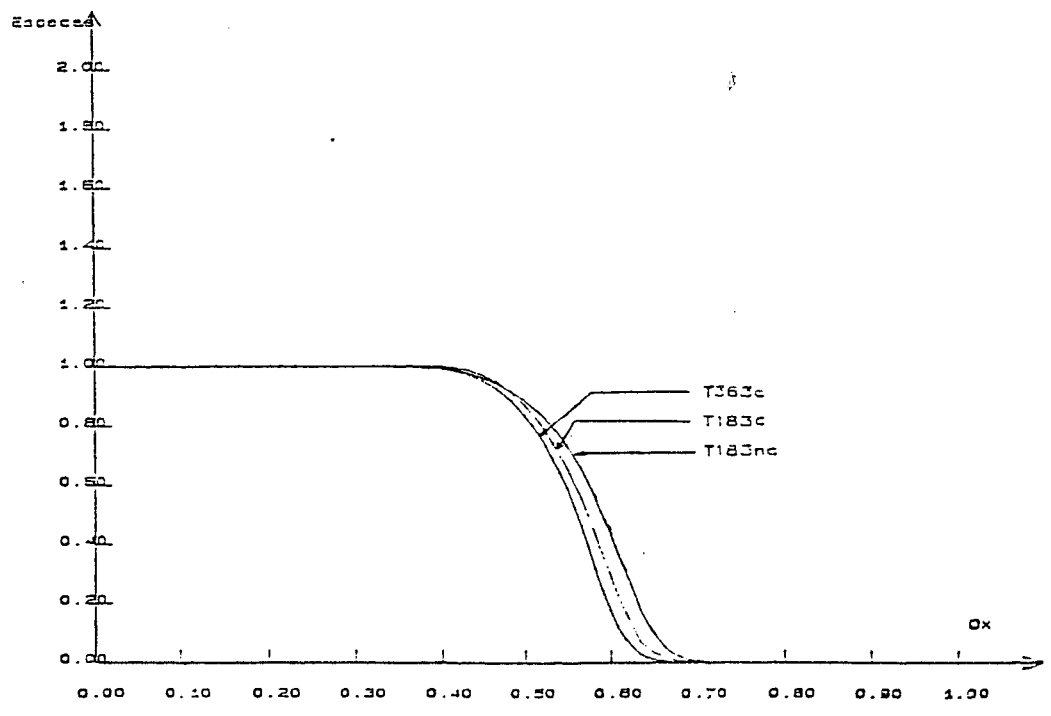

Figure 1.1.2. : mass fraction profile of reactant at t = 0.055

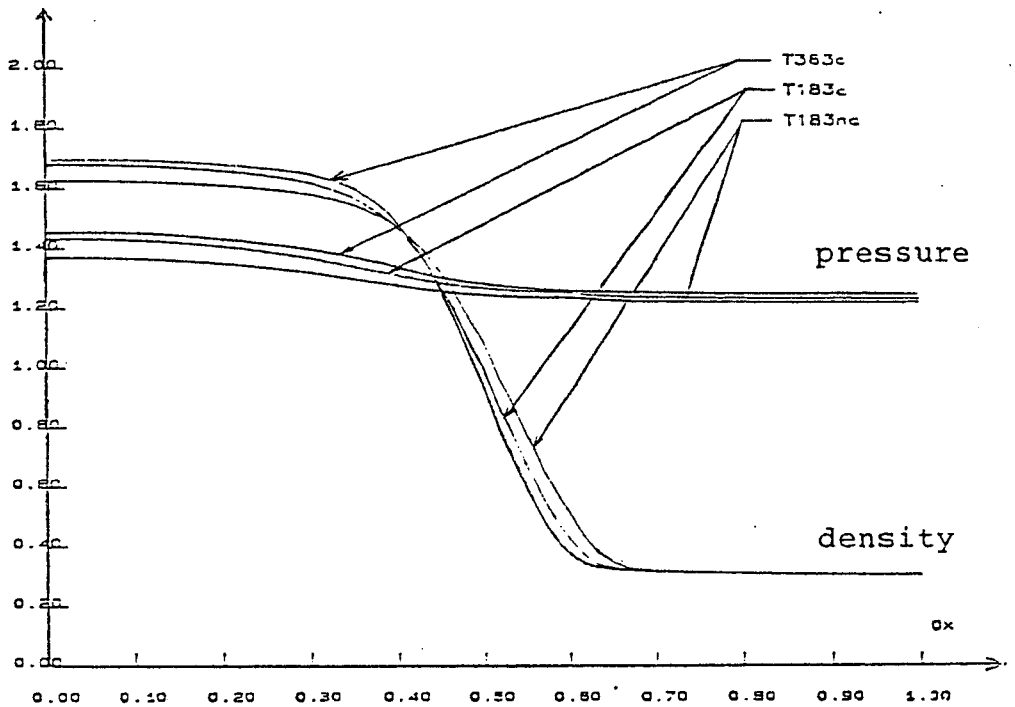

Figure 1.1.3. : pressure and density profiles at t = 0.055.

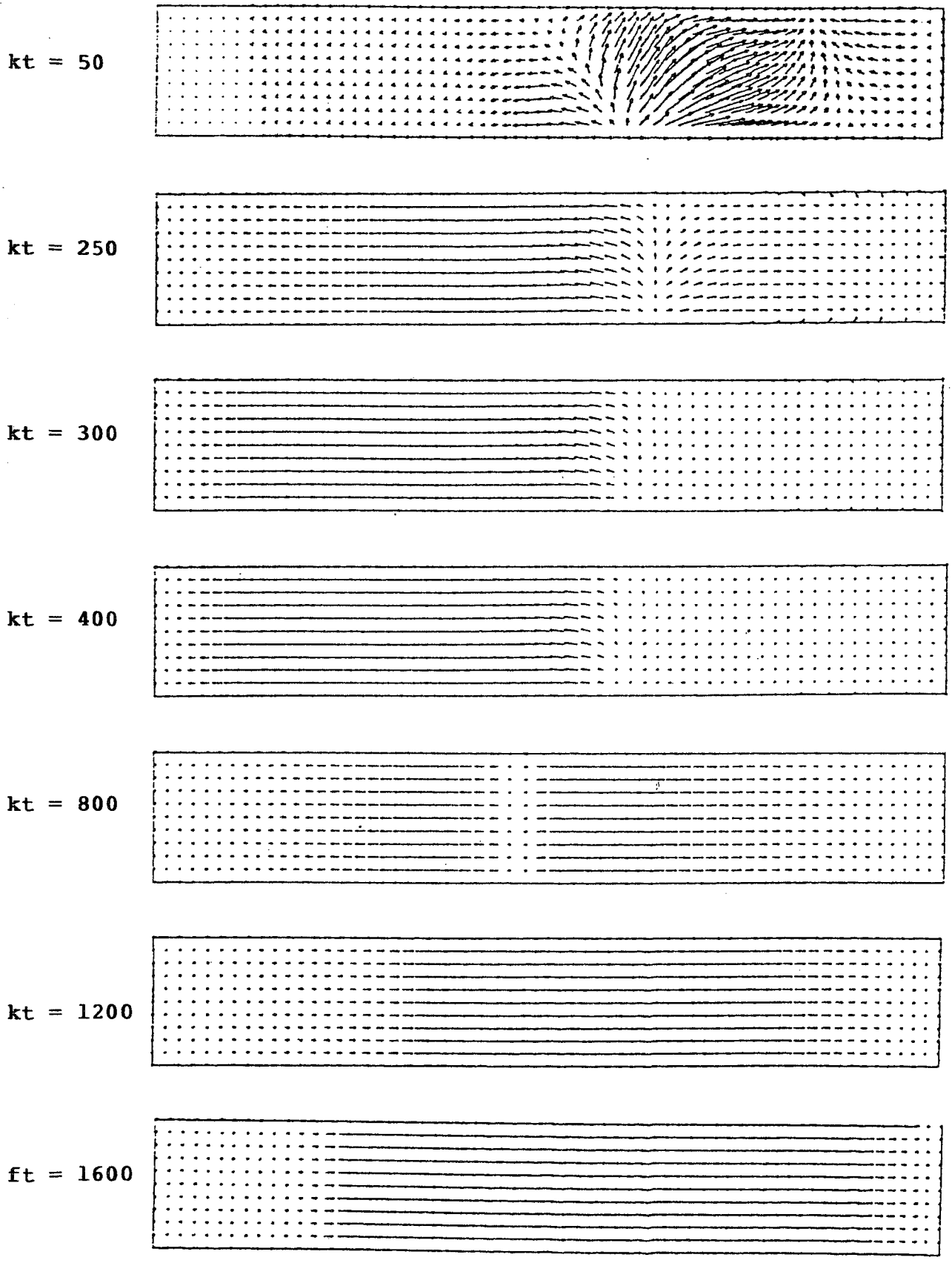

Figure 1.2.1. : Evolution of the flame,
Velocity field.

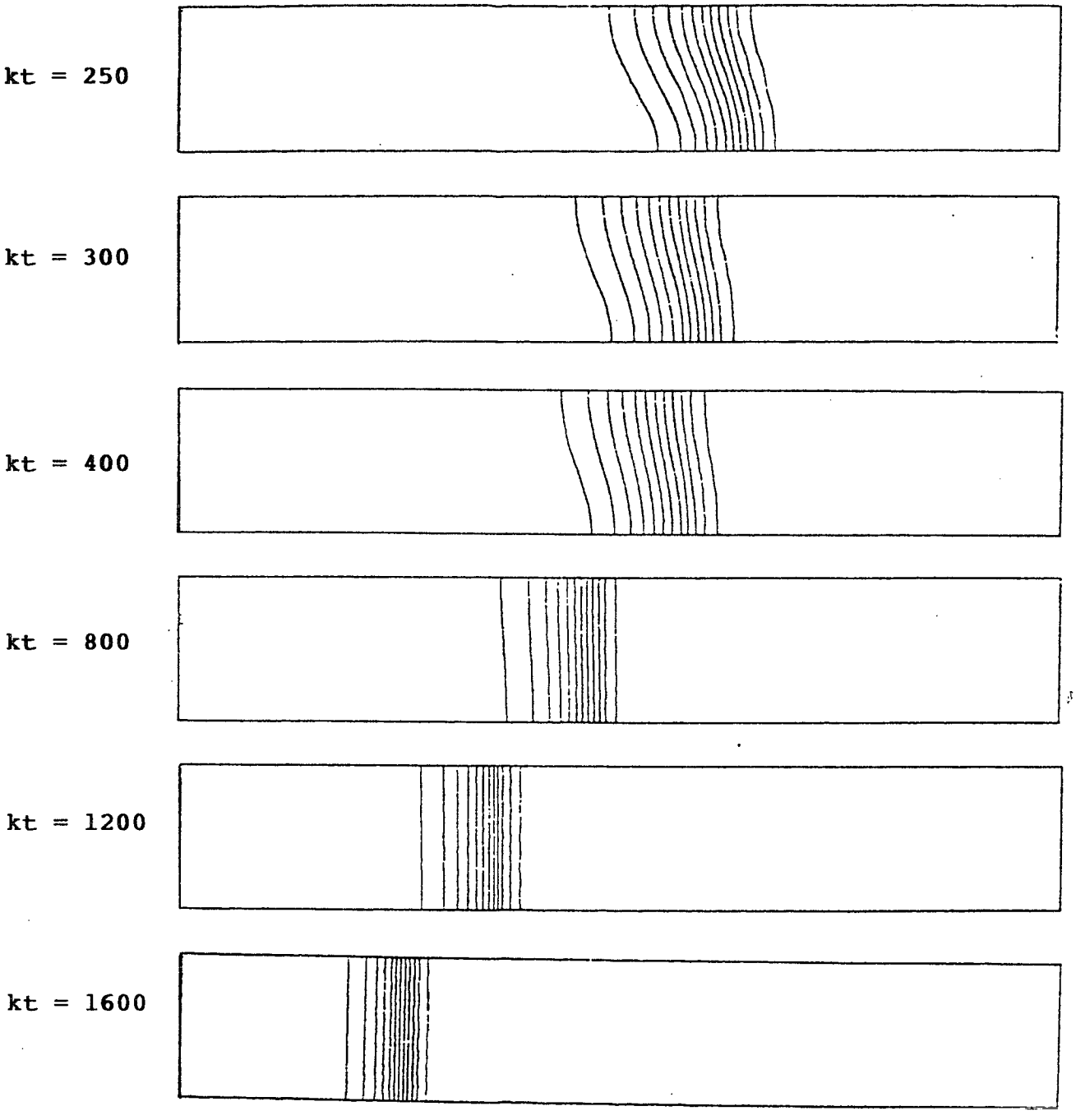

Figure 1.2.2. : Evolution of the flame,
mass fraction contours

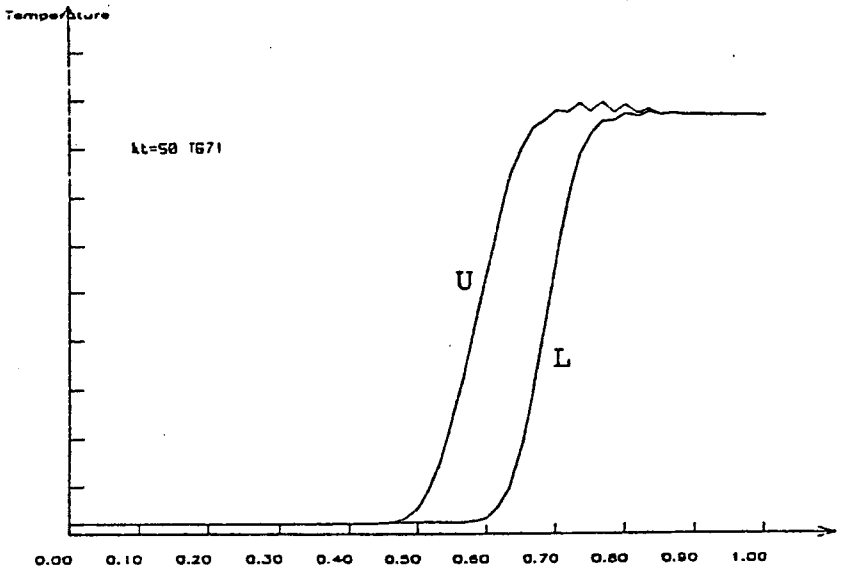

Figure 1.2.3. : Wall temperature distribution
U : Upper wall, L : Lower wall

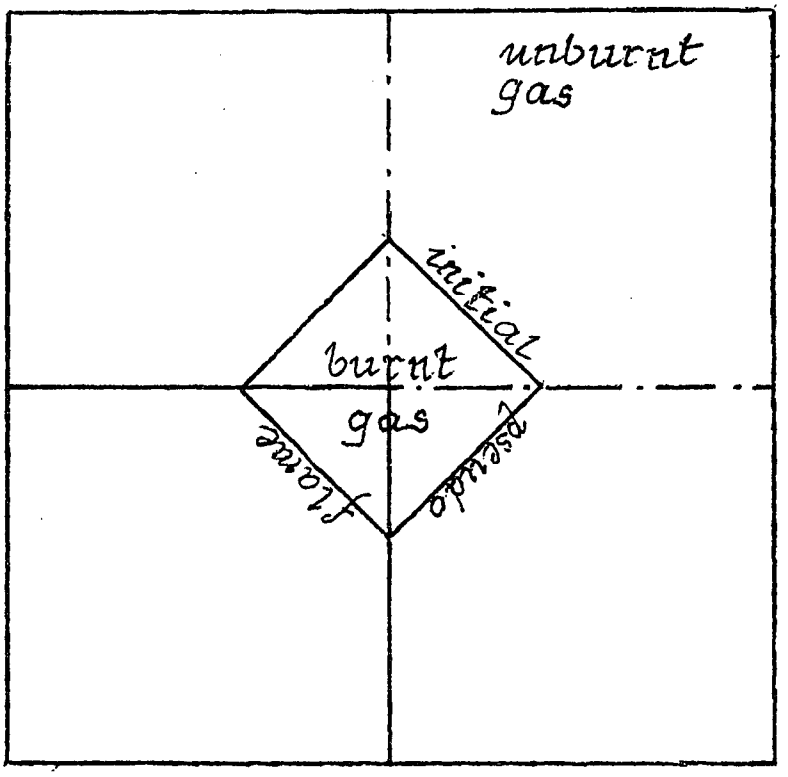

Figure 1.3.1. : Sketch of the initial configuration of the flame.

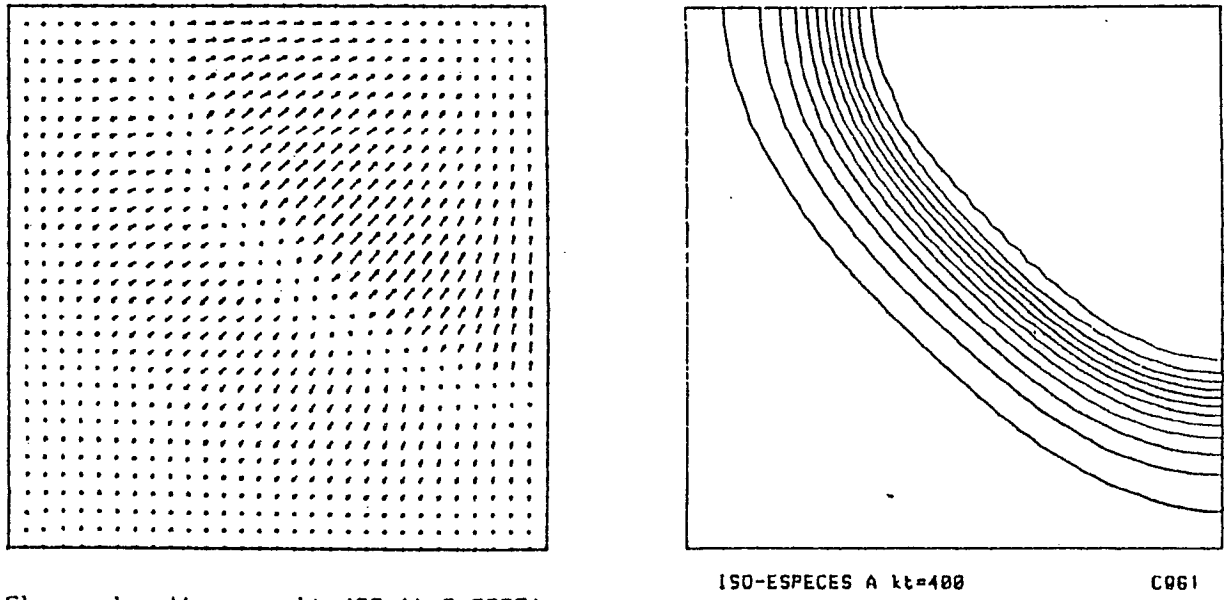

Figure 1.3.2. : Evolution of the flame
left : velocity field.
right : mass fraction contours

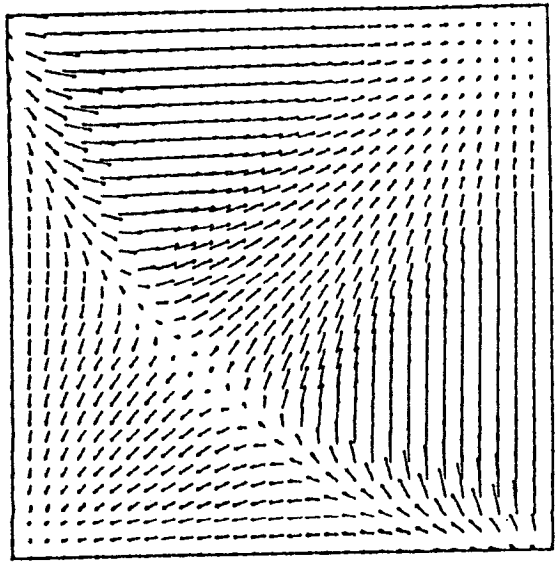

Champ de vitesse a kt=800 (t=0.0784)

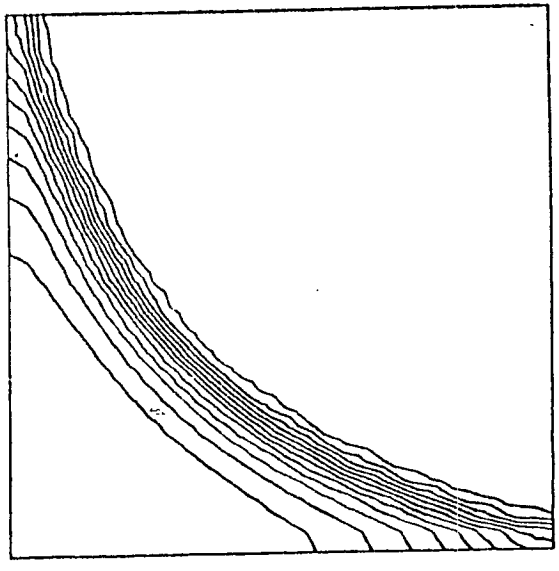

Iso-especes a kt=800 avec 15 isovaleurs.

Figure 1.3.3. : Evolution of the flame
left : velocity field
right : mass fraction contours

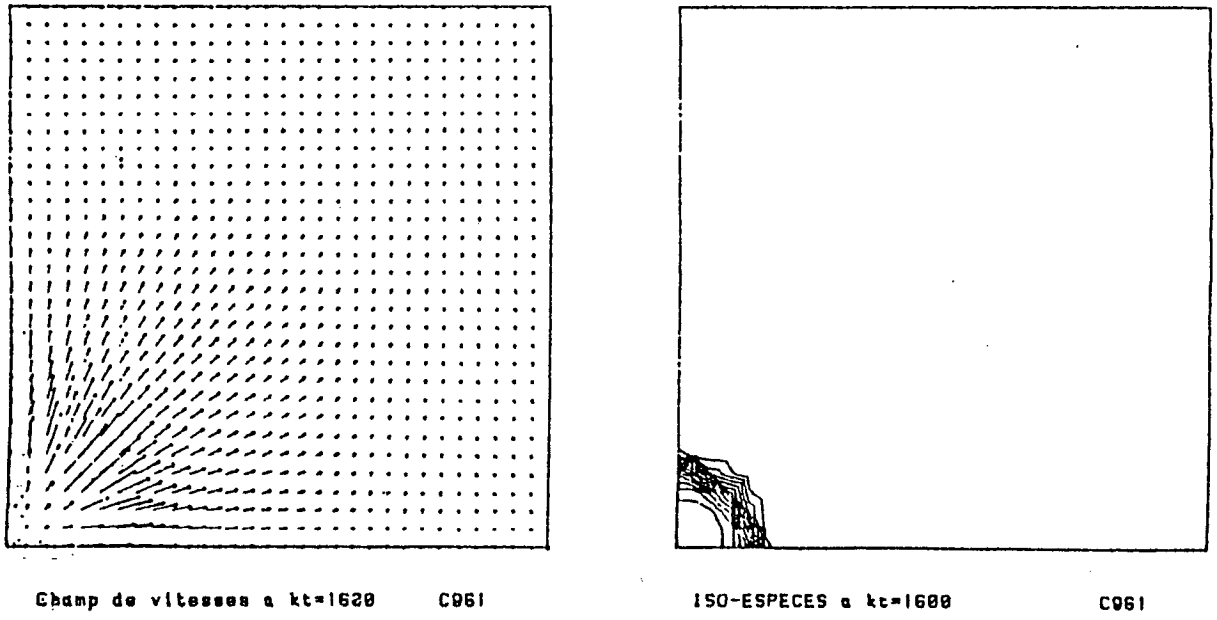

Figure 1.3.4. : Evolution of the flame
left : velocity field
right : mass fraction contours

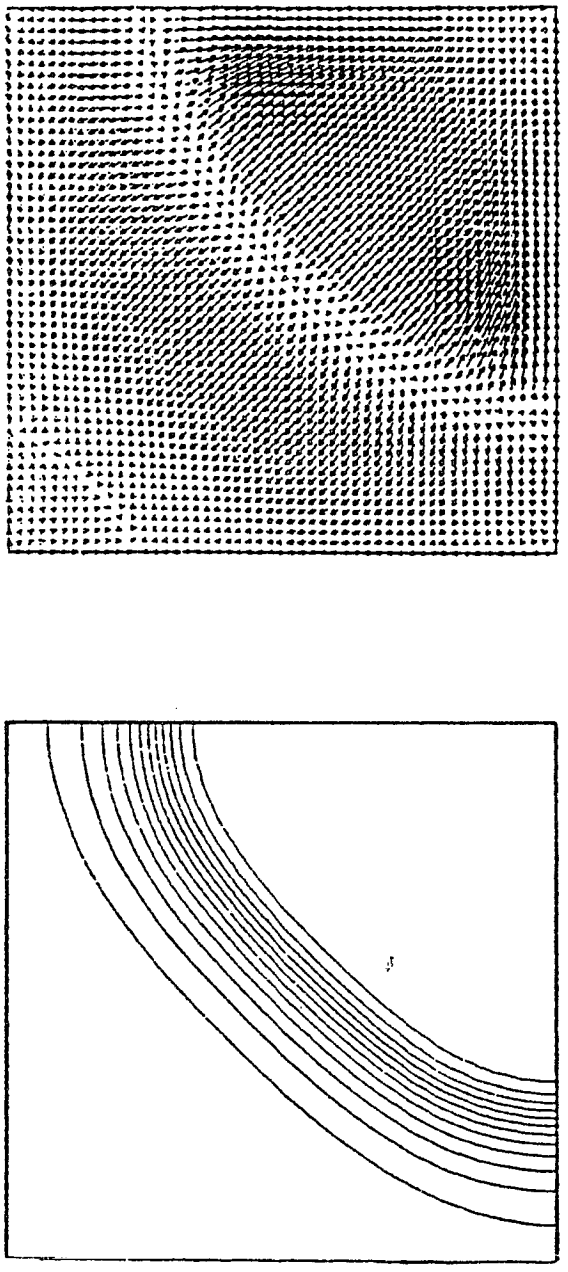

Figure 1.3.5. : Evolution of the flame
Upper plot : velocity field
Lower plot : mass fraction contours

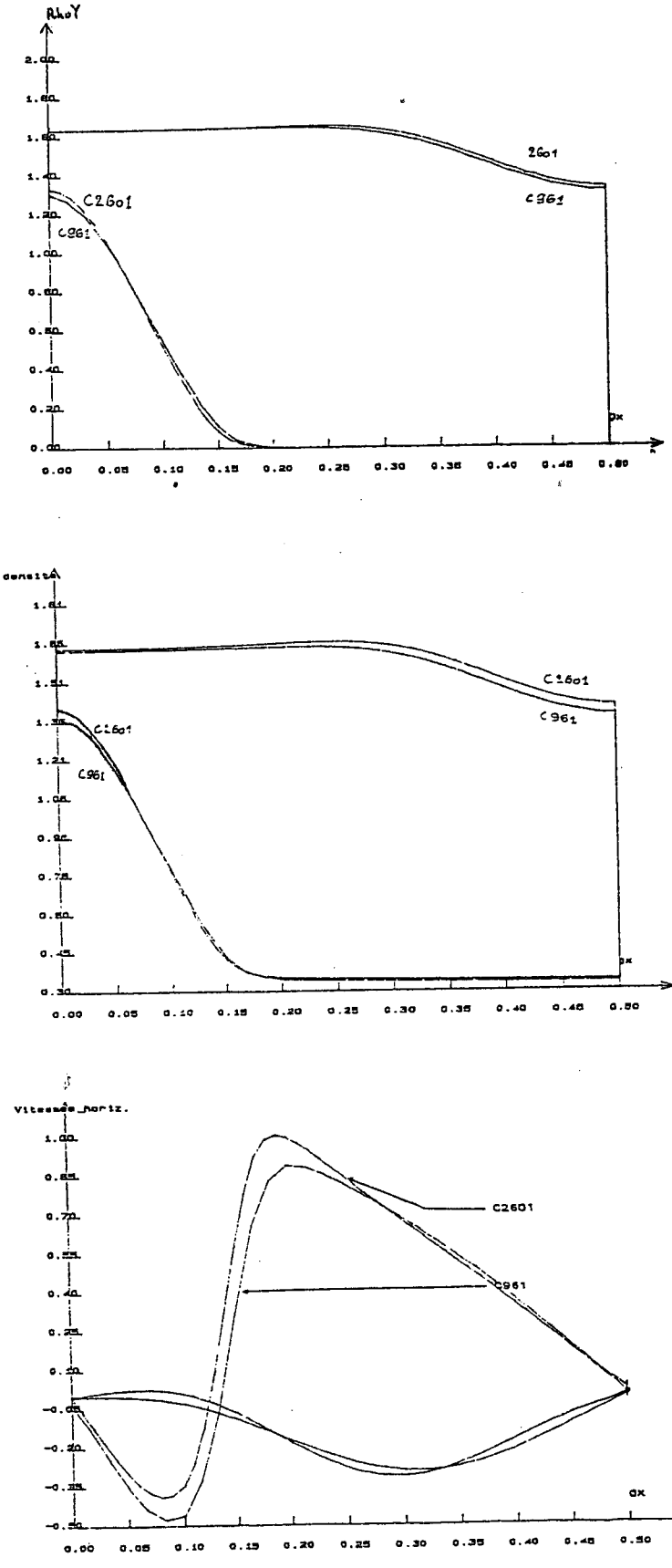

Figure 1.3.6. : Wall distribution of :
a) specie density of the reactant
b) density
c) velocity

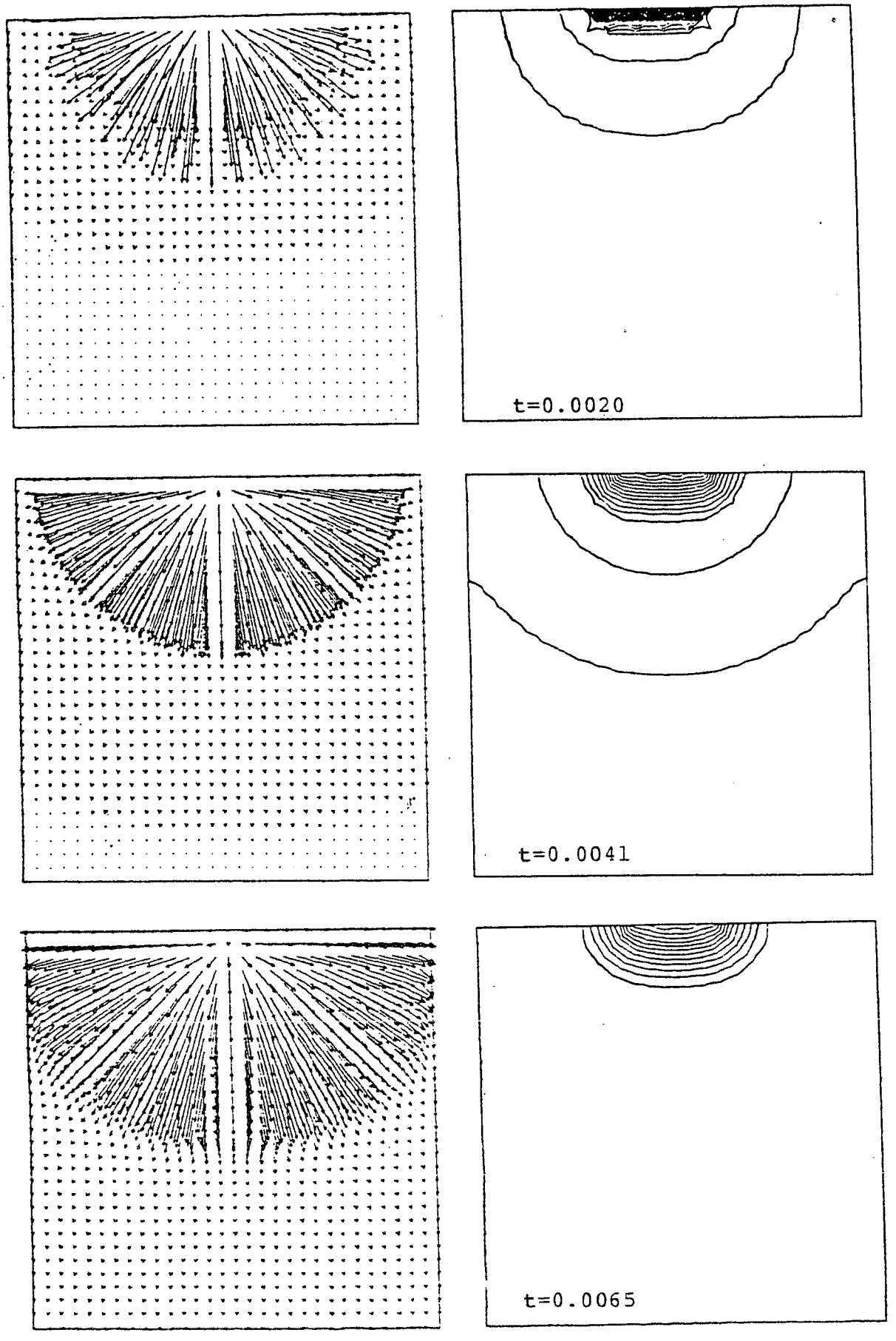

Figure 1.4.1. Evolution of the flame
left : velocity field.
right : isovalues of the mass fraction of the reactant

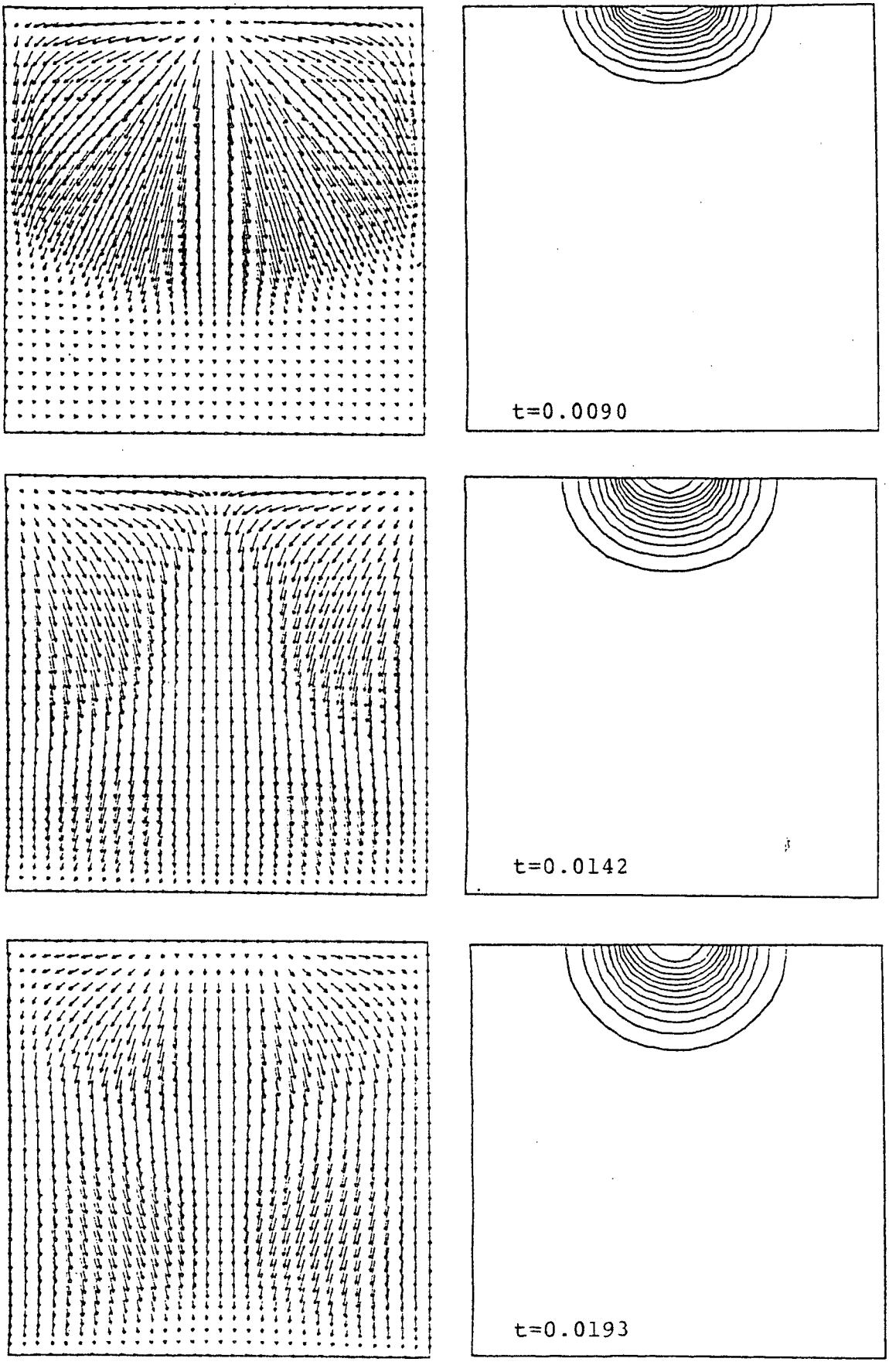

Figure 1.4.2. Evolution of the flame
left : velocity field.
right : isovalues of the mass fraction of the reactant

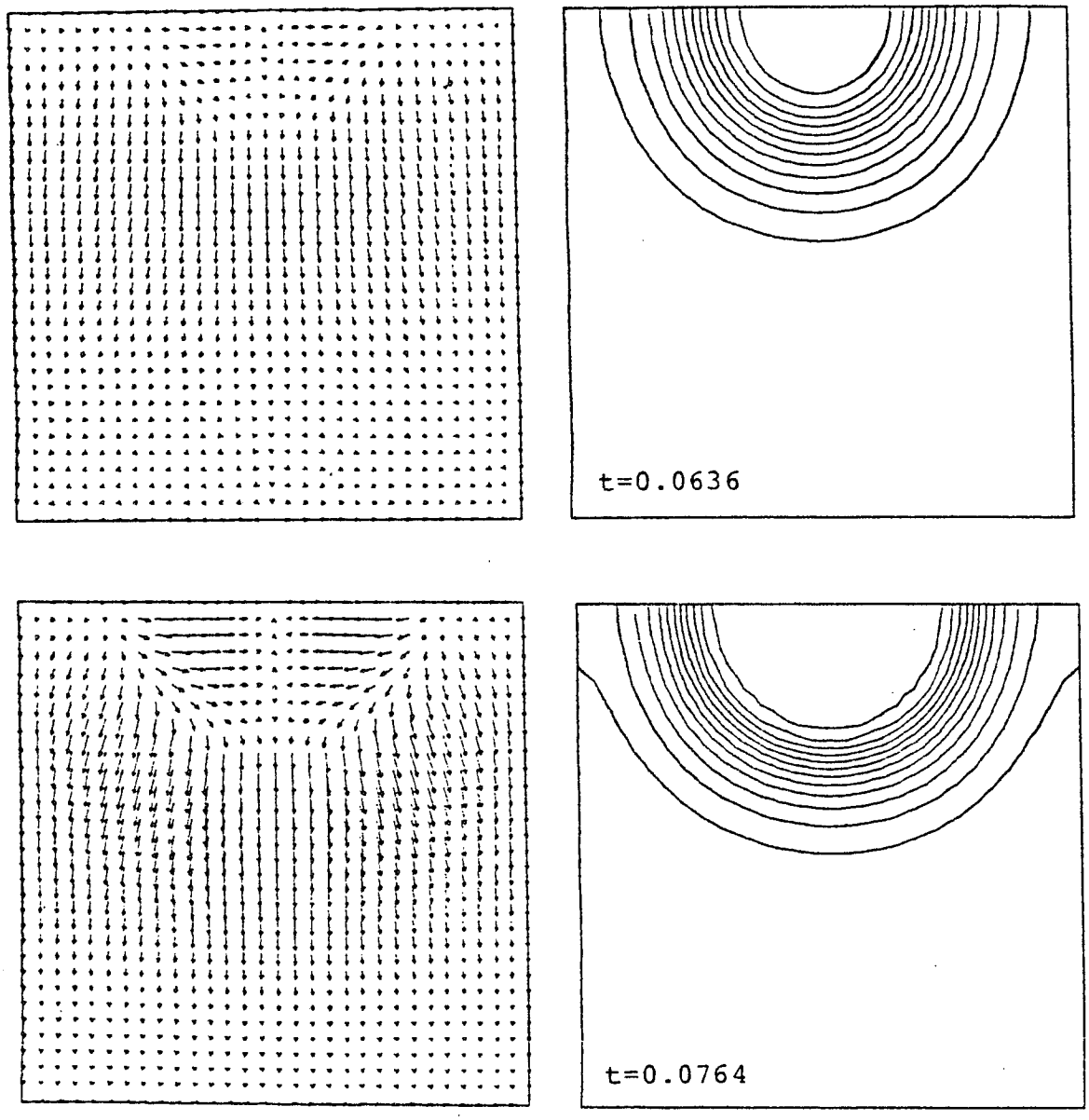

Figure 1.4.3. Evolution of the flame
left : velocity field.
right : isovalues of the mass fraction of the reactant

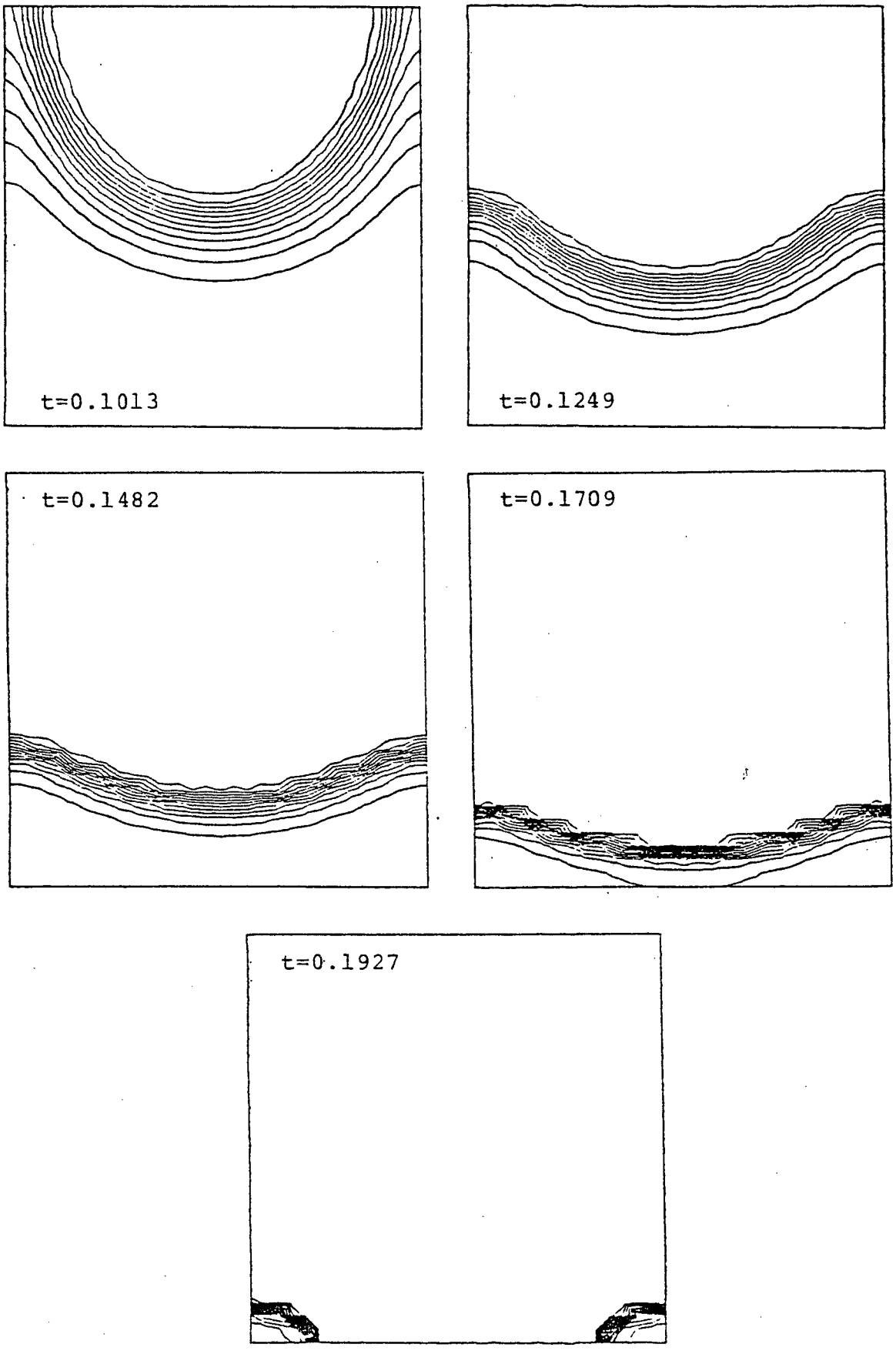

Figure 1.4.4. Evolution of the flame isovalues of the mass fraction of reactant

Figure 2.1 : Evolution of the isotherms.

kt = 100. t = 0.0037

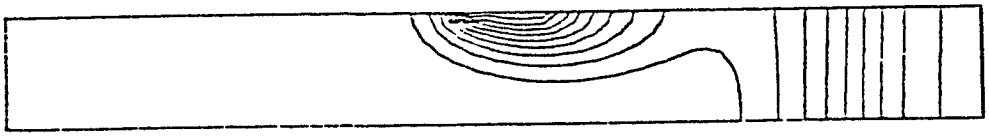

kt = 400. t = 0.0170

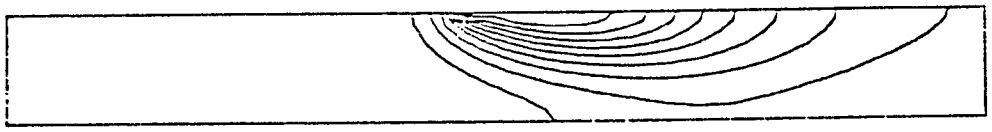

kt = 1200. t = 0.0529

kt = 2200. t = 0.0963

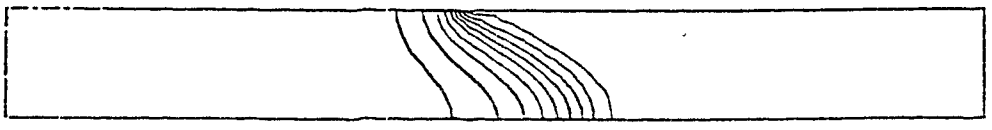

kt = 3600. t = 0.1575

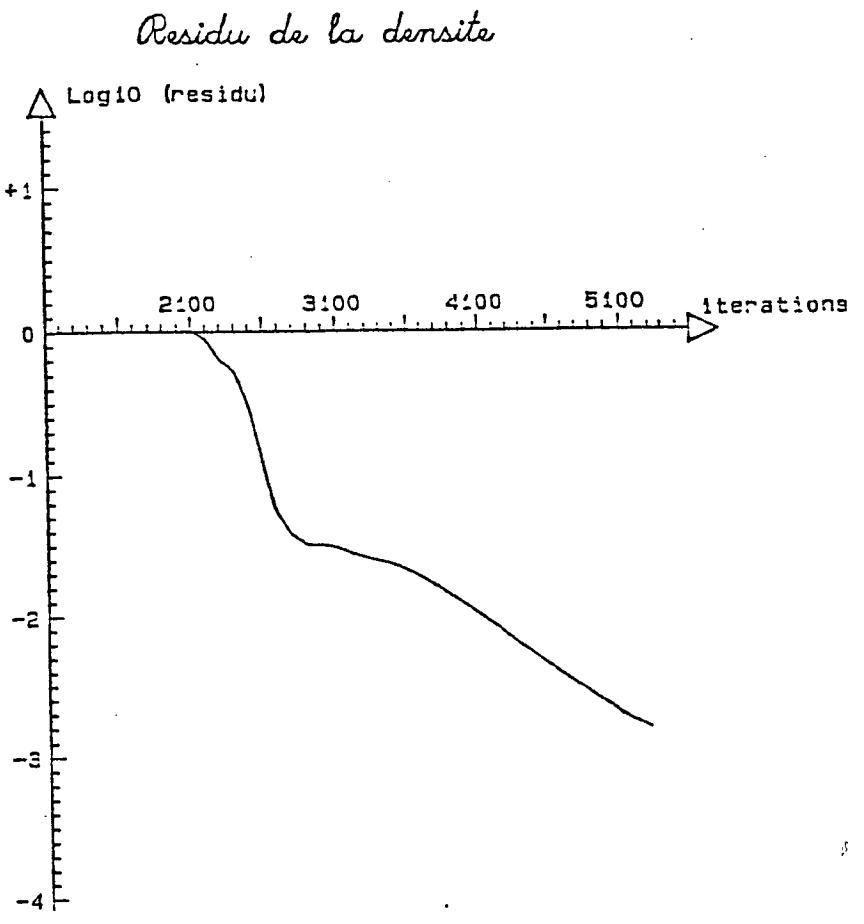

Figure 2.2. : Density residual.

Imprimé en France
par
l'Institut National de Recherche en Informatique et en Automatique